We are IntechOpen, the world's leading publisher of Open Access books Built by scientists, for scientists

4,800
Open access books available

122,000
International authors and editors

135M
Downloads

Our authors are among the

154
Countries delivered to

TOP 1%
most cited scientists

12.2%
Contributors from top 500 universities

CLARIVATE ANALYTICS BOOK CITATION INDEX INDEXED

WEB OF SCIENCE™

Selection of our books indexed in the Book Citation Index in Web of Science™ Core Collection (BKCI)

Interested in publishing with us?
Contact book.department@intechopen.com

Numbers displayed above are based on latest data collected.
For more information visit www.intechopen.com

12

Tomography Visualization Methods for Monitoring Gases in the Automotive Systems

Krzysztof Polakowski
Warsaw University of Technology
Poland

1. Introduction

Taking into consideration growing ecology and safety demands, there are a need for more accurate and cheaper ways to monitor workflows of gases, which can be used in automotive applications. Such researches come into prominence in case of more commonly applied gas systems, that use hydrocarbons as well as hydrogen, which in case of running down of oil resources, are predicated as the most probable fuel for intern combustion engines or fuel cells used in vehicles. Use of tomography can be an alternative (in relation to currently used) method for such monitoring methods. The ultrasonic flow measurement is one of the most promising. The main advantage of this method is the fact that it is based on contactless, non-invasive flow measurement which does not cause any pressure or other physics-chemical changes in observed environment.

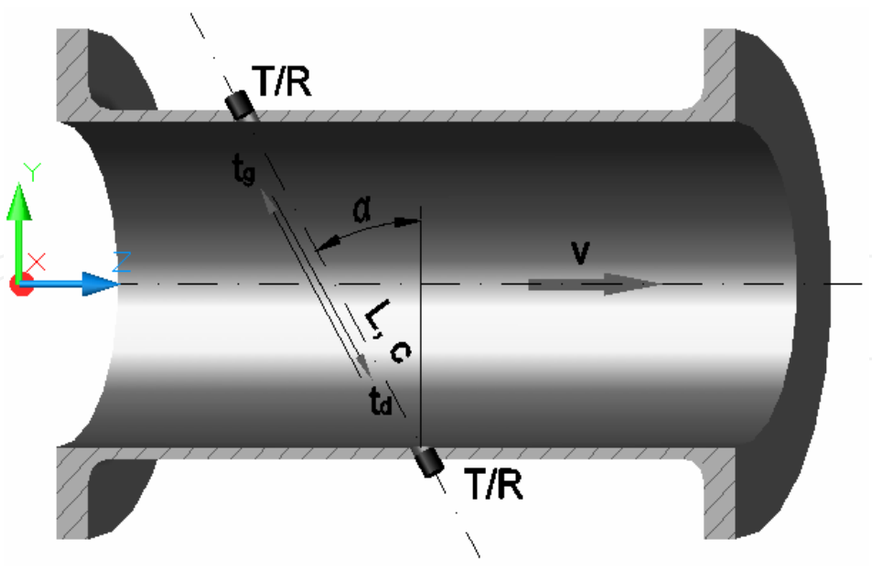

Fig. 1. A scheme of the ultrasonic transit-time flowmeter

The measurement principle of an ultrasonic transit-time flowmeter involves at least one pair of ultrasonic transducers: transmitter (T) and receiver (R). Transmitting transducers are triggered to send an ultrasonic pulse, one upstream and one downstream to the receiving

transducers. Due to the fact that the distance between the opposite arranged transducers L is known, the travel time of the pulses can be estimated if the temperature is also known. The measurement principle of an ultrasonic transit-time flowmeter utilizes an ultrasonic travel time measurement for the calculation of both velocity v of the flowing medium and the speed of sound c (Kupnik, 2008):

$$v = \frac{L}{2\sin(\alpha)} \frac{t_g - t_d}{t_g t_d} \tag{1}$$

and

$$c = \frac{L}{2} \frac{t_g + t_d}{t_g t_d} \tag{2}$$

In general, the measure of the matter that moves in a given time through a given transport cross-section is termed flow rate. The matter can be in solid, liquid or gaseous form. I should distinguish between volumetric flow rate Q_v (quantity of a flow in cubic metre per unit time) and mass flow rate Q_m (quantity of a flow in kilograms per unit time) (Kupnik, 2008):

$$Q_v = \frac{dV}{dt} = v_A A \tag{3}$$

and

$$Q_m = \frac{dm}{dt} = \rho Q_v = \rho v_A A \tag{4}$$

where V is the volume, m is the mass, A is the cross-section of the transport way, v_A is the averaged velocity over cross-sectional area of the transport way and ρ is the density.
A fundamental problem in acoustic flow measurement is the fact that the distribution of the velocity in the measurement pipe in each case is not known exactly, because an ultrasonic transit-time flowmeter always determines the averaged velocity along the sound path (v_s), i.e. it integrates the velocity profile over the volume of the sound beam. Exact knowledge of the velocity profile is essential to convert the line averaged path velocity v_s to the velocity v_A. The connection between these two velocities is usually considered by a correction factor k_v, also termed meter factor (Kupnik, 2008):

$$k_v = \frac{v_A}{v_S} \tag{5}$$

For a given axially symmetric flow profile v(r), where r denotes the radius and D denoted the internal diameter of the pipe, can write (Kupnik, 2008):

$$k_v = \frac{v_A}{v_S} = \frac{4}{D} \frac{\int_0^R v(r)\, r\, dr}{\int_0^R v(r)\, dr} \tag{6}$$

Equation (6) shows clearly that meter factor k_v.depends directly on the flow profile $v(r)$. Each deviation of the flow profile from the assumed one, which is used in Equation (6), forcibly leads to uncertainties of the flowmeter. Finding an appropriate model equation for the flow profile $v(r)$ for each flow measurement problem is essential (Kupnik, 2008).
Multipath systems with different sets of emitters and receivers are used in order to enlarge the data and accuracy of measurement (Mandard at al., 2008). In considered system equally spaced sensors around the pipe's perimeter in perpendicular surface to pipe's axis were placed. In the system the transmitters one by one generates ultrasound impulses, which with different delays reach all receivers. The time duration of these waves is the basis for calculation of the average value of measured flow's speed (Roger & Baker, 2005).
If I assume that the transmitters emit ultrasound waves of not too high frequencies, than the angle of spreading groups of waves is big enough to allow them to reach all of the receivers placed in pipe's perimeter (Opieliński at al., 2006).
The speed profile image (a magnitude of speed vectors distribution on the surface perpendicular to flow direction) we can achieve with an aid of ultrasonic tomography method.

2. The inverse problem solution

New generations of computer's tomography systems often based on algebraic algorithms of image reconstruction (ART) from projections. The tomography image is constructed with the help of algorithm, which digitize the diagnosed area to the quadratic cells, which geometric centres are handled like pixels of the image.
Velocity profile image construction in a plane of receivers means estimation of a set of unknown values, which we can denote as $f(x, y)$.
I can get integrated values of speed on a base of time measurement of ultrasonic impulses travelling like rays from transmitters to the receivers (Fig. 2). These values, according to projection method, are named the ray-sum measured with i-th ray s_i. I have assumed that in each cell of the rectangular or square grid, the function $f(x, y)$ is constant. The relationship between the f_j's and s_i's may be expressed as:

$$\sum_{j=1}^{n} w_{ij} f_j = s_j, \quad i = 1,2,...,m \tag{7}$$

where: m is total number of rays (main and auxiliary ones) in all projections, n number of cells crossed by rays, w_{ij} is the weighting factor that represents the contribution of the j-th cell to the i-th ray integral.
The iterative method, based on the "method of projections" as first proposed by Kaczmarz (Kak & Slaney, 1999) is very useful for solving this problem. In this method a grid representation with n^2 cells gives image of n degrees of freedom. Therefore, an image, represented by (f_1, f_2, …, f_n) may be considered to be a single point in an n dimensional space. In this space each of equations (8), represents a hyperplane. When a unique solution of these equations exists (for $m \geq n$), the intersection of all these hyperplanes is a single point giving that solution.
The equation (7) we can write in an expanded form:

$$\begin{aligned} &w_{11}f_1 + w_{12}f_2 + w_{13}f_3 + \cdots + + w_{1n}f_n = s_1 \\ &w_{21}f_1 + w_{22}f_2 + w_{23}f_3 + \cdots + + w_{2n}f_n = s_2 \\ &\vdots \\ &w_{m1}f_1 + w_{m2}f_2 + w_{m3}f_3 + \cdots + + w_{mn}f_n = s_m \end{aligned} \tag{8}$$

In order to solve the system of equations (8) we have used least squares method which gives an excellent results particularly in case when m is bigger than n (over-determined system of equations).

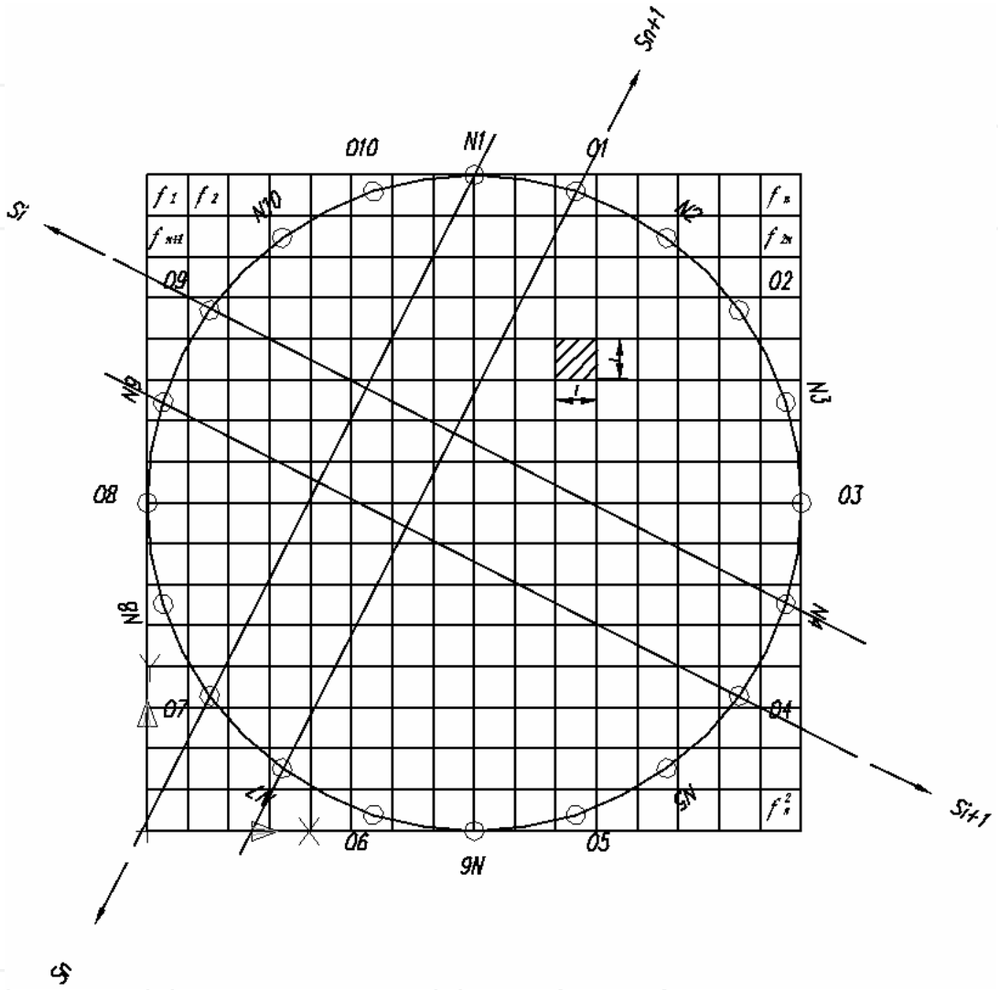

Fig. 2. A square grid and the rays in the cross-section of the transport way

If n and m were small we could use conventional matrix theory methods to invert the system of equations (1). For larger values m and n may have to be used some least squares method for solving this problem (Lawson at al., 1995).

I'm looking for set of solutions of $[f_1, f_2, \ldots, f_n]$ which equally well satisfy all of equations (8), but every value s_i is measured with an error. So, in order to solve this problem we should to look for a global minimum in an n–dimensional space, for example with the help of the least squares method.

The factors w_{ij} of the cells, which are not crossed by the rays are equal to 0. When a j-th cell is crossed by i-th ray this factor could be calculated according to very simple relation (9):

$$w_{ij} = \frac{\sqrt{2}}{lp_{ij}} \tag{9}$$

Problem of image construction in case of the ultrasonic flowmeters very often leads to the over determined algebraic set of equations (2), which in matrix form can be expressed:

$$\boldsymbol{W}\boldsymbol{f} = \boldsymbol{s} \tag{10}$$

where: $\boldsymbol{W}$ is the matrix of dimensions $m \times n$ and $m > n$, $\boldsymbol{s}=[s_1,s_2,\ldots,s_m]$ – right hand side vector, and $\boldsymbol{f}=[f_1,f_2,\ldots f_n]^T$ – the solution vector. One of the ways of the solution of the problem (8) is to find the vector $\boldsymbol{f}^*$, which minimize Euclidean norm of residual vector $\mathbf{r}$ for the known matrix $\boldsymbol{W}$ and vector $\boldsymbol{s}$. It means: $\|\boldsymbol{r}\|_2=min\|\boldsymbol{s}-\boldsymbol{W}\boldsymbol{f}\|_2$, $\|\boldsymbol{f}^*\|_2=min\|\boldsymbol{f}\|2$,
where - the last minimum is taken for all vectors $\boldsymbol{f}$ which fulfil the previous relation. This is Linear Least Squares Problem (LSP) (Lawson at al., 1995).
In order to calculate the solution to Problem LS and analyzing the effect of data errors as they influence to it, we will use the Singular Value Decomposition (SVD) theorem. This theorem says that for any arbitrary matrix $\boldsymbol{W}\in R_{m\times n}(m \geq n)$ of pseudo-rank k exists an m by m orthogonal matrix $\boldsymbol{U}\in R_{m\times n}$ an n by n orthogonal matrix $\boldsymbol{V}\in R_{m\times n}$ and $\boldsymbol{D}\in R_{m\times n}$ such that:

$$\boldsymbol{W} = \boldsymbol{U}\boldsymbol{D}\boldsymbol{V}^T \tag{11}$$

where:

$$\boldsymbol{D} = \begin{bmatrix} d_1 & 0 & 0 & 0 \\ 0 & d_2 & 0 & 0 \\ . & . & . & . \\ 0 & 0 & 0 & d_n \end{bmatrix} \in R_{m\times n} \tag{12}$$
$$d_1 \geq d_2 \geq d_k > d_{k+1} = d_{k+2} = \cdots d_n = 0$$

and k is the pseudo-rank of matrix $\boldsymbol{W}$.
The diagonal entries $d_i$of the diagonal matrix $\boldsymbol{D}$ are known as singular values of matrix $\boldsymbol{W}$ and relation (11) as a Singular Value Decomposition (SVD), (Polakowski at al., 2007, a).
This decomposition is closely related to the eigenvalue-eigenvector decomposition of the symmetric nonnegative matrix $\boldsymbol{W}^T\boldsymbol{W}$, and diagonal terms of matrix $\boldsymbol{D}$ are the squared eigenvalues of $\boldsymbol{W}^T\boldsymbol{W}$. Columns of matrix $\boldsymbol{V}$ are the orthonormal eigenvectors of $\boldsymbol{W}^T\boldsymbol{W}$, and columns of matrix $\boldsymbol{U}$ are eigenvectors of $\boldsymbol{W}\boldsymbol{W}^T$.
Knowing the Singular Value Decomposition (11) one can easily to find the solution of LSP:

$$\boldsymbol{f}^* = \boldsymbol{W}^+\boldsymbol{s} \tag{13}$$

where: $\boldsymbol{W}^+=\boldsymbol{V}\boldsymbol{D}^+\boldsymbol{U}^T$ is the pseudoinverse of matrix $\boldsymbol{W}$ (or inverse matrix in Moore – Penrose sense) and $\boldsymbol{D}^+ = diag\left(\frac{1}{d_1},\ldots,\frac{1}{d_k},0,\ldots,0\right) \in R_{m\times n}$.

For a square nonsingular matrix $\boldsymbol{W}$, the pseudoinverse of matrix $\boldsymbol{W}$ is the inverse of matrix $\boldsymbol{W}$.

$$\boldsymbol{W}^+ = \boldsymbol{W}^{-1} \tag{14}$$

In case of ill-conditioned problem (in tomography usually we have to deal with ill-conditioned problems) the solution can be achieved in the following way. Suppose the singular value decomposition is computed for the matrix $\boldsymbol{W}$:

$$\boldsymbol{W} = \boldsymbol{U}\begin{bmatrix}\boldsymbol{D}\\0\end{bmatrix}\boldsymbol{V}^T \tag{15}$$

One can compute:

$$\boldsymbol{g} = \boldsymbol{U}^T\boldsymbol{s} \tag{16}$$

and consider the least squares problem:

$$\begin{bmatrix}\boldsymbol{D}\\0\end{bmatrix}\boldsymbol{q} \cong \boldsymbol{g} \tag{17}$$

where $\boldsymbol{q}$ is related to $\boldsymbol{f}$ by the orthogonal linear transformation:

$$\boldsymbol{f} = \boldsymbol{V}\boldsymbol{q} \tag{18}$$

Problem (18) is equivalent to the problem $\boldsymbol{W}\boldsymbol{f} \cong \boldsymbol{s}$ in the sense of general orthogonal transformations of least squares problems. Since $\boldsymbol{D}$ is diagonal ($\boldsymbol{D}=diag\{d_1,d_2,\ldots,d_n\}$) the effect of each component of $\boldsymbol{q}$ upon the residual norm is immediately obvious. Introducing a component q_j with the value:

$$q_j = \frac{g_j}{d_j} \tag{19}$$

reduces the sum of squares of residuals by the amount q_j^2.

Assume the singular values are ordered so $d_k \geq d_{k+1}$, k=1,2,…,n. It is then natural to consider "candidate" solutions for problem (18) of the form:

$$\boldsymbol{q}^{(k)} = \begin{bmatrix}q_1\\\vdots\\q_k\\0\\\vdots\\0\end{bmatrix} \quad k = 0,1,\ldots,n \tag{20}$$

where q_j is given by Eq. (19). The candidate solution vector $\boldsymbol{q}^{(k)}$ is the pseudoinverse solution (i.e., the minimal length solution) of problem (18) under the assumption that the singular values d_j for $j \geq k$ are regarded as being zero.

From the candidate solution vectors $\boldsymbol{q}^{(k)}$ one obtains candidate solution vectors $\boldsymbol{f}^{(k)}$ for the problem $\boldsymbol{W}\boldsymbol{f} \cong \boldsymbol{s}$ as:

$$\boldsymbol{f}^{(k)} = \boldsymbol{V}\boldsymbol{q}^{(k)} = \sum_{j=1}^{k} q_j V^j, \qquad k = 0,\ldots,n \tag{21}$$

where V^j denotes the j-th column vector of $\boldsymbol{V}$.

Note that:

$$\left\|\boldsymbol{r}^{(k)}\right\|^2 = \left\|\boldsymbol{q}^{(k)}\right\|^2 = \sum_{j=1}^{k} q_j^2 = \sum_{j=1}^{k}\left(\frac{q_j}{d_j}\right)^2 \tag{22}$$

hence $\left\|\boldsymbol{f}^{(k)}\right\|$ is a nondecreasing function of k.
The squared residual norm associated with $\boldsymbol{f}^{(k)}$ is given by:

$$\left\|\boldsymbol{r}^{(k)}\right\|^2 = \left\|\boldsymbol{s} - \boldsymbol{W}\boldsymbol{f}^{(k)}\right\|^2 = \sum_{j=k+1}^{m} g_j^2 \tag{23}$$

Inspections of the columns of the matrix $\boldsymbol{V}$ associated with small singular values are a very effective technique for identifying the set of columns of $\boldsymbol{W}$ that are nearly linearly dependent.
Suppose that the matrix $\boldsymbol{W}$ is ill-conditioned; then some of the later singular values are significantly smaller than the earlier ones. In such a case some of the later q_j values may be undesirably large. One hopes to locate an index k such that all coefficients q_j for $j \le k$ are acceptably small, all singular values d_j for $j \le k$ are acceptably large, and the residual norm $\boldsymbol{r}^{(k)}$ is acceptably small. If such an index k exists, then one can take the candidate vector $\boldsymbol{f}^{(k)}$ as an acceptable solution vector. (Polakowski at al., 2007, b).
In order to choose a preferred value of index k one can use a graph of residual norm versus solutions norm $\left\|\boldsymbol{r}^{(k)}\right\| = f\left(\left\|\boldsymbol{f}^{(k)}\right\|\right)$. For ill-conditioned problems we have „L" shaped curve. Using such the graph it is easy to determine the optimal value of index k.
Using the method called FOCUSS (FOCal Underdetermined System Solver) we could solve a system of underdetermined algebraic set of equations (fewer measurements than the unknowns which are a common case for industrial tomography), (Gorodinitsky at al., 1995).
It let us consider the following constrained optimization problem
Minimize

$$\boldsymbol{J}_p(\boldsymbol{f}) = p\,|\,fj\,| \tag{24}$$

subject to

$$\boldsymbol{W}\boldsymbol{f} = \boldsymbol{s}$$

where f_j are non zero values of the matrix $\boldsymbol{f}$ and $\boldsymbol{J}_p(\boldsymbol{f})$ (often called the diversity measure) is some measure of sparsity of signals and it can take form, called the generalized p-norm :

$$\boldsymbol{J}_p(\boldsymbol{f}) = sign(p)\sum_{j=1}^{n} p\,|\,f_j\,|^p \tag{25}$$

where $p \le 1$ and is selected by the user.
To minimize the generalized p norm diversity measure $\boldsymbol{J}_p(\boldsymbol{f})$ in (21), subject to the equality constraint $\boldsymbol{W}\boldsymbol{f} = \boldsymbol{s}$ we define the Lagrangian $\boldsymbol{L}(\boldsymbol{f},\boldsymbol{\lambda})$ as:

$$\boldsymbol{L}(\boldsymbol{f},\boldsymbol{\lambda}) = \boldsymbol{J}_p(\boldsymbol{f}) + \boldsymbol{\lambda}(\boldsymbol{s} - \boldsymbol{W}\boldsymbol{f}) \tag{26}$$

where $\boldsymbol{\lambda} \in R^n$ is a vector of Lagrange multipliers and $\boldsymbol{D}_{|f|} \in R^{(n\times n)}$ is a diagonal matrix with the entries $d_j = |f_j|^{2-p}$.

Solving the above equations by simple mathematical operations, we obtain that

$$\lambda_* = |p| \left(\boldsymbol{W} \boldsymbol{D}_{|f|}(\boldsymbol{f}_*) \boldsymbol{W}^T \right) - 1 \boldsymbol{s} \tag{27}$$

$$\boldsymbol{f}_* = |p|^{-1} \boldsymbol{D}_{|f|}(\boldsymbol{f}_*) = \boldsymbol{D}_{|f|}(\boldsymbol{f}_*) \boldsymbol{W}^T (\boldsymbol{W} \boldsymbol{D} | \boldsymbol{f}_* | \boldsymbol{W}^T)^{-1} \boldsymbol{s} \tag{28}$$

The equation (24) is not in a convenient form for computation since the desired vector $\boldsymbol{f}_*$ is implicitly in the right side of the equation $\boldsymbol{f}_*$. However, it suggests that an iterative algorithm for estimation of the optimal vector $\boldsymbol{f}_*$ is given as:

$$\boldsymbol{f}(k+1) = \boldsymbol{D}_{|f|}(k) \boldsymbol{W}^T (\boldsymbol{W} \boldsymbol{D}_{|f|}(k) \boldsymbol{W}^T)^{-1} \boldsymbol{s} \tag{29}$$

where

$$\boldsymbol{D}_{|f|}(k) = diag\{ | f_1(k) |^{2-p}, | f_2(k) |^{2-p}, | f_n(k) |^{2-p} \} \tag{30}$$

The above algorithm, called the generalized FOCUSS algorithm can be expressed in a more compact form:

$$\boldsymbol{f}(k+1) = \tilde{\boldsymbol{D}}_{|f|}(k) [\boldsymbol{W} \tilde{\boldsymbol{D}} | f | (k)]^+ \boldsymbol{s} \tag{31}$$

where the superscript $(.)^+$ denotes the Moore-Penrose pseudo-inverse and

$$\tilde{\boldsymbol{D}}_{|f|}(k) = \boldsymbol{D}_{|f|}^{1/2}(k) = diag\{ | f_1 |^{1-p/2}(k), | f_2 |^{1-p/2}(k), | f_n |^{1-p/2}(k) \} \tag{32}$$

It's should be noted that the matrix $\boldsymbol{D}_{|f|}$ exists for all f and even for a negative p. For p=2, the matrix $\boldsymbol{D}_{|f|} = \boldsymbol{J}$ and the FOCUSS algorithm simplifies to the standard LS or the minimum 2-norm solution:

$$\boldsymbol{f}_* = \boldsymbol{W}^T (\boldsymbol{W} \boldsymbol{W}^T)^{-1} \boldsymbol{s} \tag{33}$$

3. Results

The system of equations describing the tomographic flowmeter was solved with the aid of Linear Least Squares method for overdetermined algebraic set of equations. With the method called FOCUSS (FOCal Underdetermined System Solver) I have solved a system of underdetermined algebraic set of equations.

Condition number of the resulting rectangular matrix was high enough so that the classical Kaczmarz's algorithm was not able to produce correct results. That's why I have to take into account pseudo rank deficiency of the matrix coefficients. I have considered all possible candidate solutions, when k was changing from 1 till the full pseudo – rank equal to 1000 (Polakowski at al., 2008, a).

The images and their relief plots constructed on the basis of the candidate solutions are presented in Figure: 4b, 6b and 7b. The images and their relief plots constructed on the basis of FOCUSS are presented in Figure: 4c, 5b, c, d, 6c and 7c.

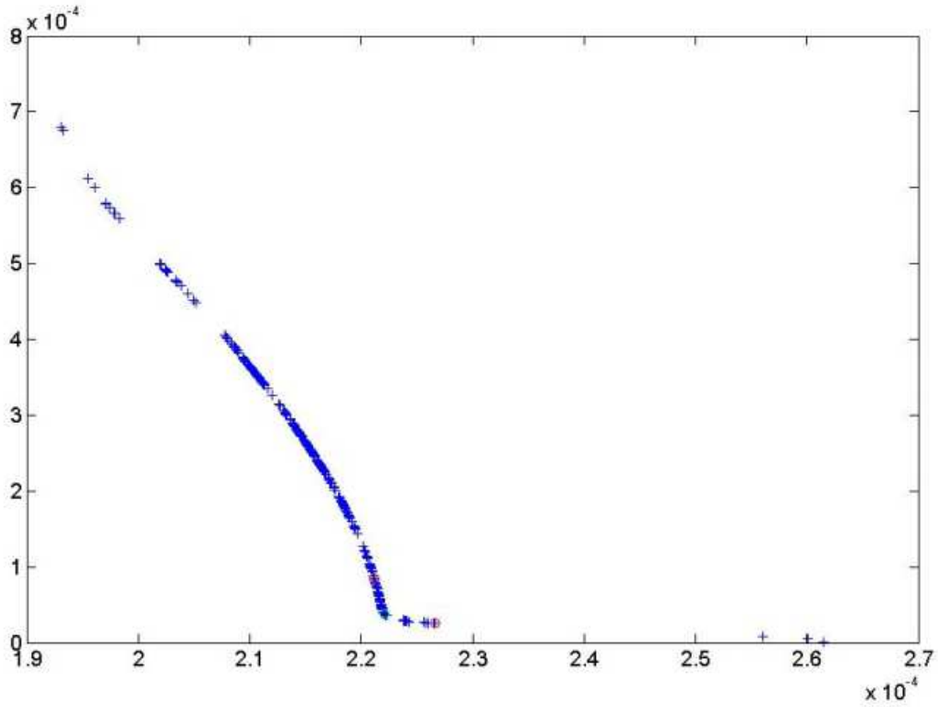

Fig. 3. Diagram $\|\boldsymbol{r}^{(k)}\| = f(\|\boldsymbol{f}^{(k)}\|)$ of the residual vector norm versus the solution vector norm for the cross shaped object

	The resolution of grid 16x16, number of the rays 256	The resolution of grid 16x16, number of the rays 624
a)	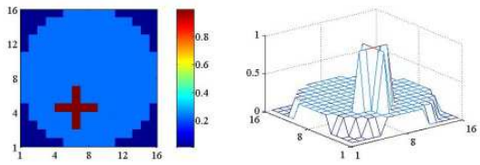	
b)	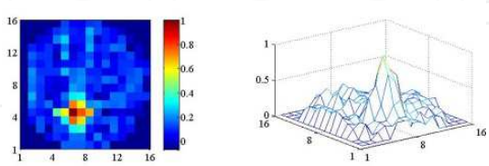	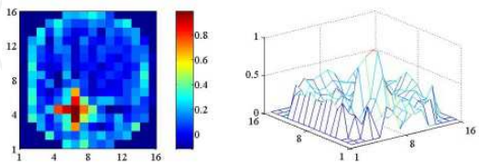
c)	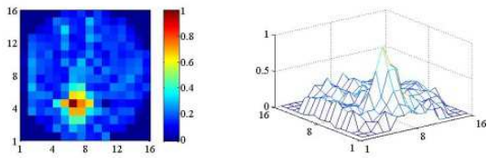	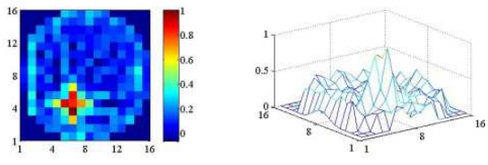

Fig. 4. The changes of images and the relief plots of a cross shaped object in dependence of number of the rays a) reconstructed object, b) reconstruction with the aid of Linear Least Squares Method , c) reconstruction with the aid of FOCUSS

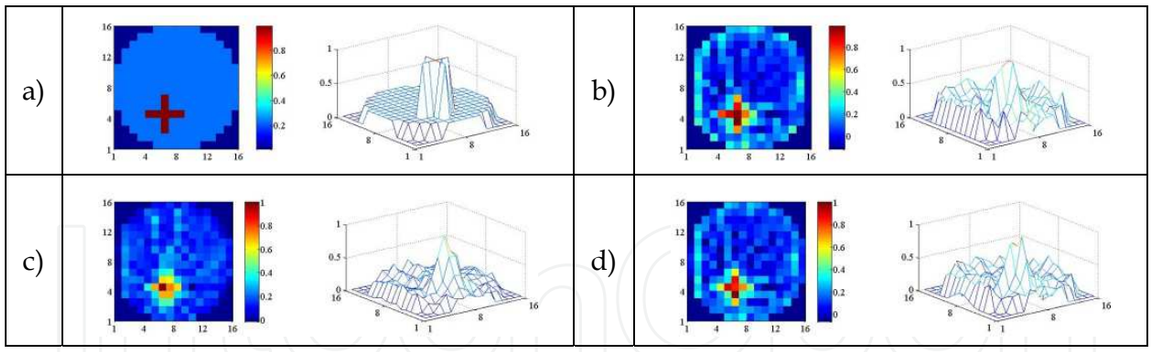

Fig. 5. Images and the relief plots of a cross shaped object reconstructed with the aid of FOCUSS in dependence of regularity index a) reconstructed object, b) regularity index 0.02 , c) regularity index 0.2, d). regularity index 50.

When I compare Figure: 5b, c and d we can also see, that the images have not been improved with the bigger regularization parameter, when the resolution of the grid was not to high.

Inspecting those images we can observe the influence of the resolution of the square greed and number of the rays on the object forming inside the region. The influence of resolution and number of the rays on improving the image we can clearly see on Figure 4, 5, 6 and 7.

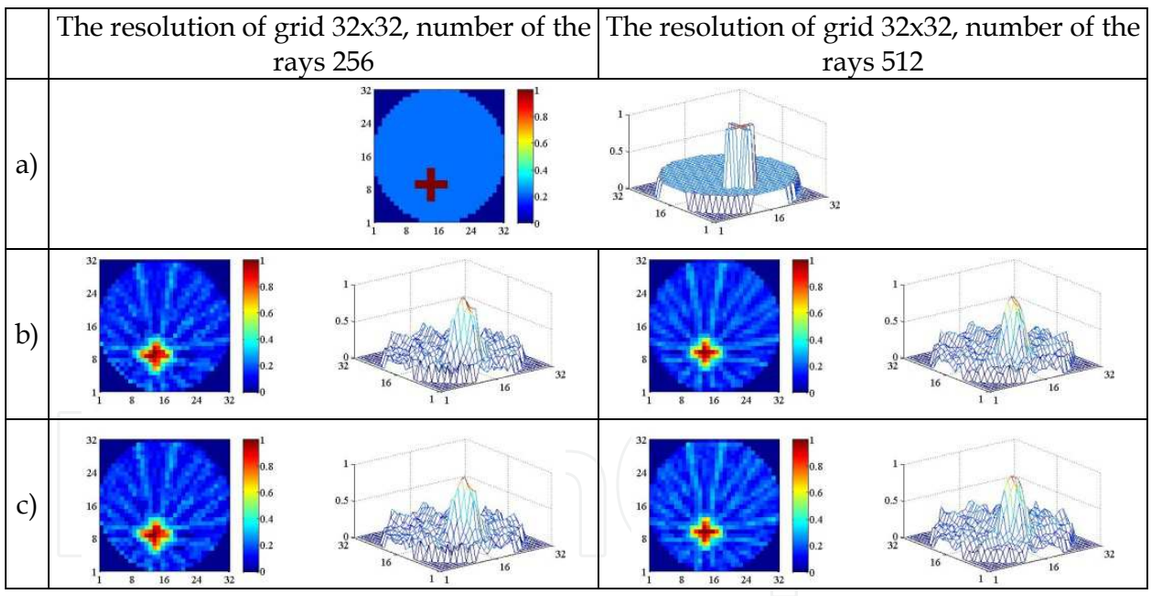

Fig. 6. The changes of images and the relief plots of a cross shaped object in dependence of number of the rays a) reconstructed object, b) reconstruction with the aid of Linear Least Squares Method , c) reconstruction with the aid of FOCUSS

It is worth to mention, that shown in Figures: 4÷7 achieved results were constructed for unpolluted synthetic data and the images were not filtered in order to check the behaviour of the image construction algorithm.

Theoretical and experimental researches carried out in this work prove that by increasing the number of radiuses which cross the pipe we increase the number of rows in the coefficient matrix ***W***. It causes the results improvement, but at the same algorithm's

	The resolution of grid 64x64, number of the rays 256	The resolution of grid 64x64, number of the rays 512
a)	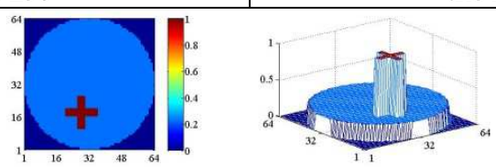	
b)	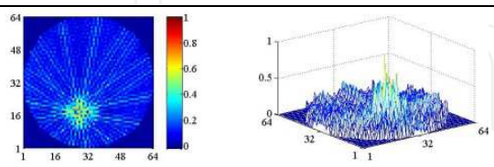	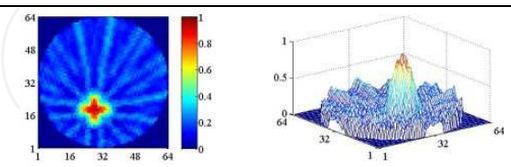
c)	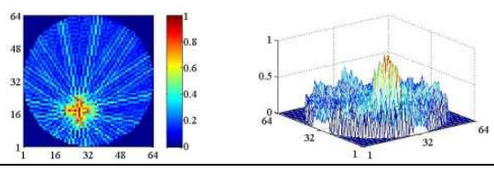	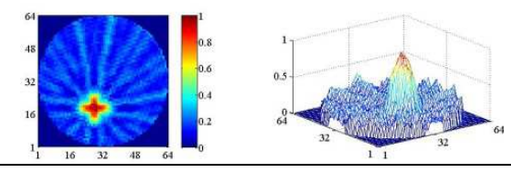

Fig. 7. The changes of images and the relief plots of a cross shaped object in dependence of number of the rays a) reconstructed object , b) reconstruction with the aid of Linear Least Squares Method , c) reconstruction with the aid of FOCUSS

execution time. Thus the number of rays should be selected in reasonable and considered way, thinking about image's quality and algorithm's execution time. By increasing the size of the resolution of the square greed (increase number of pixel) we cause a rise of the number of columns in coefficient matrix ***W***. On the other hand, with higher resolution of the square greed, reconstructed object could have more details and it is more similar to the real object. We should notice that with higher resolution of the square greed, the number of rays has to be increased proportionally.

After checking the behaviour of described above the image construction algorithms we tried to receive a velocity profile of the flow. For receive a velocity profile computations were made in area of a pipe with 0,20 m diameter. In the model transmitters (N=32) and receivers (O=48) were evenly distributed around cross-sectional area of the pipe as shown in Fig. 8.

In analyzed model the transmitters one by one generates ultrasound impulses, which with different delays reach all receivers (Polakowski at al., 2008, b).

This work contains examples of simulation computations of the complex shape modelling the flow with complicated 3D shape (Fig. 9). Chosen methods made it possible to obtain tomographic images that accurately map tested shape (Fig. 11).

The tested area with modelled object was divided into 5 surfaces (Fig. 10). In each surface were made 32 projections with help of 32 x 48 rays between 32 transmitters and 48 receivers in each surface. In all surfaces were made calculations, which gave tomography images of calculated area. On figure 9 are shown only 9 from all achieved results with their relief plots.

From these 2,5 D results we can quite accurately reconstruct the whole 3D modelled flow shape.

The system of equations describing that tomographic imaging was solved with the aid of Linear Least Squares Method. Condition number of the resulting rectangular matrix was high enough so that the classical Kaczmarz's algorithm was not able to produce correctly

results (Polakowski at al., 2008, b). That is why I have to take into account pseudo rank deficiency of the matrix coefficients. I have considered all possible candidate solutions according Eq. (21), when k was changing from 1 till the full pseudo–rank.

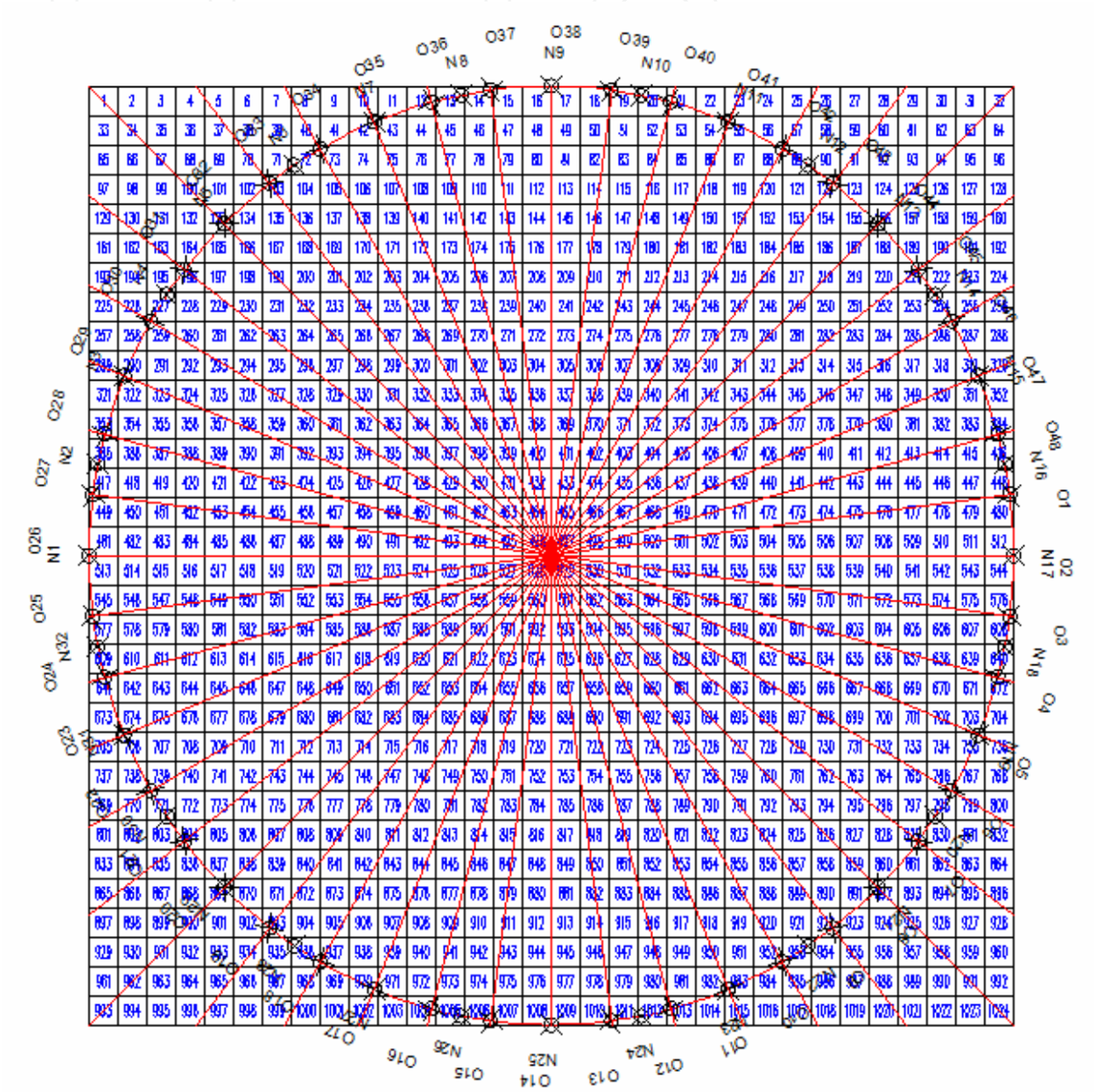

Fig. 8. Modelled area divided with 32x32 pixels and evenly distributed transducers: 32 transmitters N x 48 receivers O

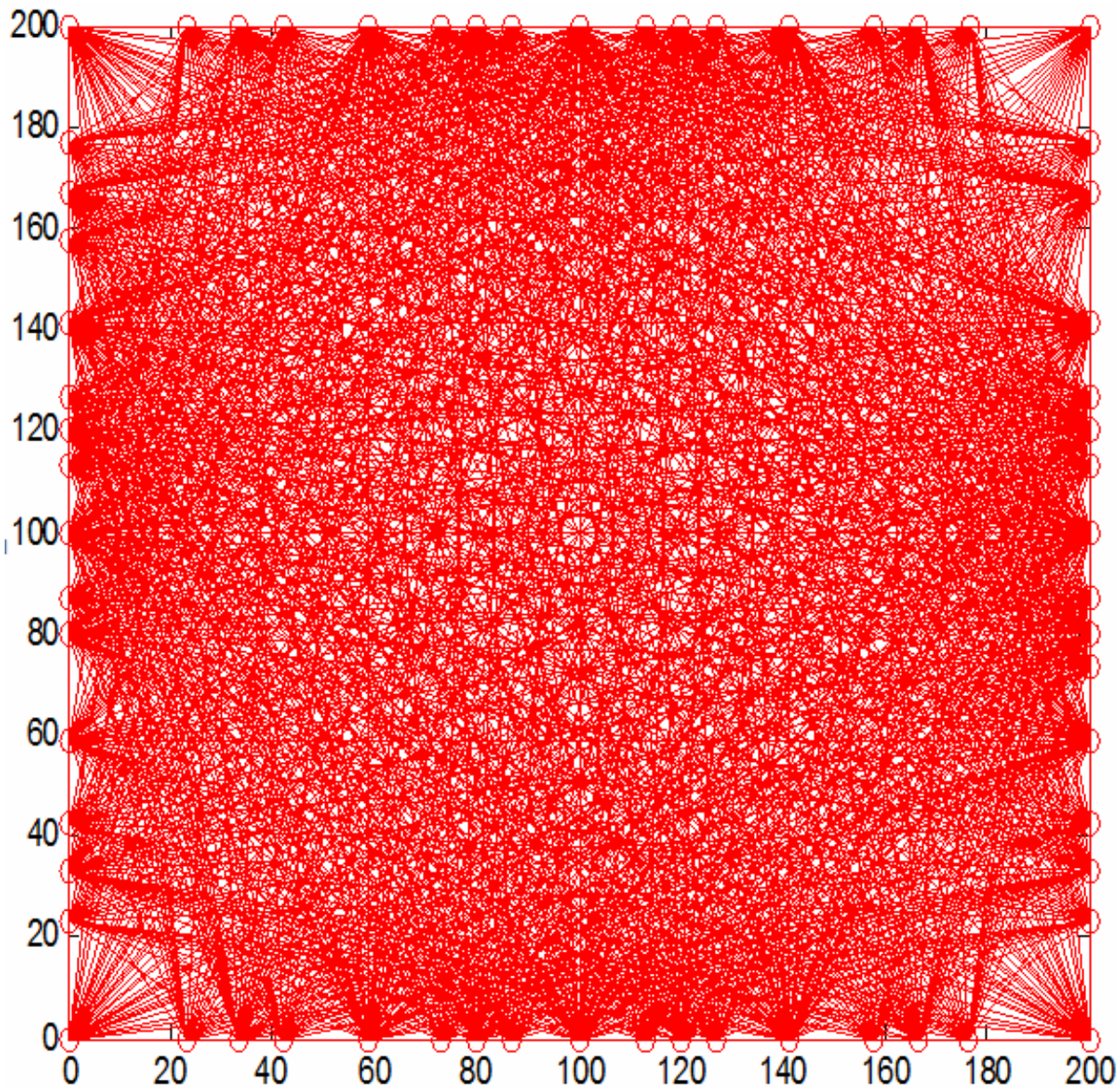

Fig. 9. All possible 1536 rays in modelled cross-sectional area from 32 projections between 32 transmitters and 48 receivers

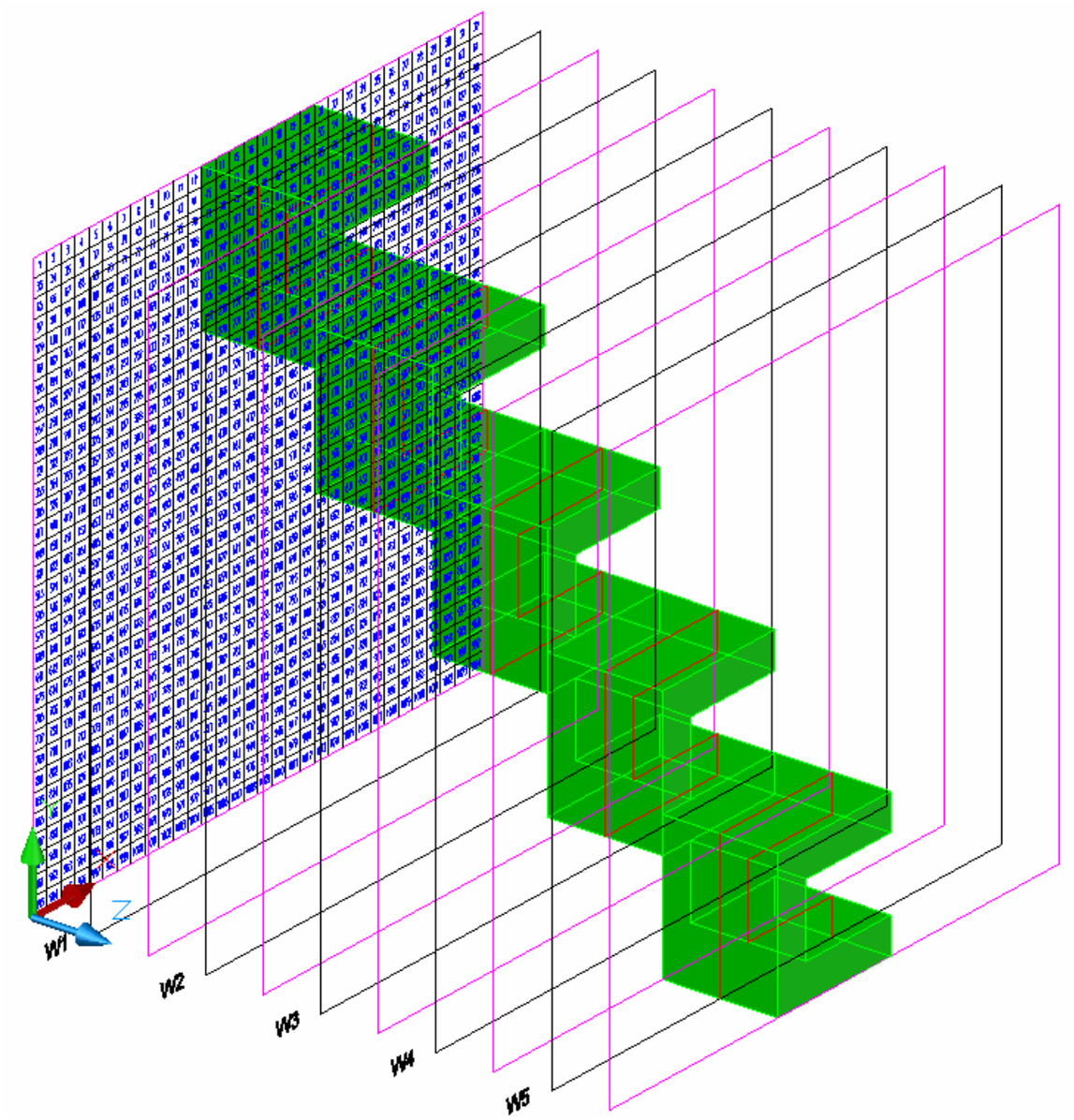

Fig. 10. Model of the complicated flow shape and its 2,5D visualization

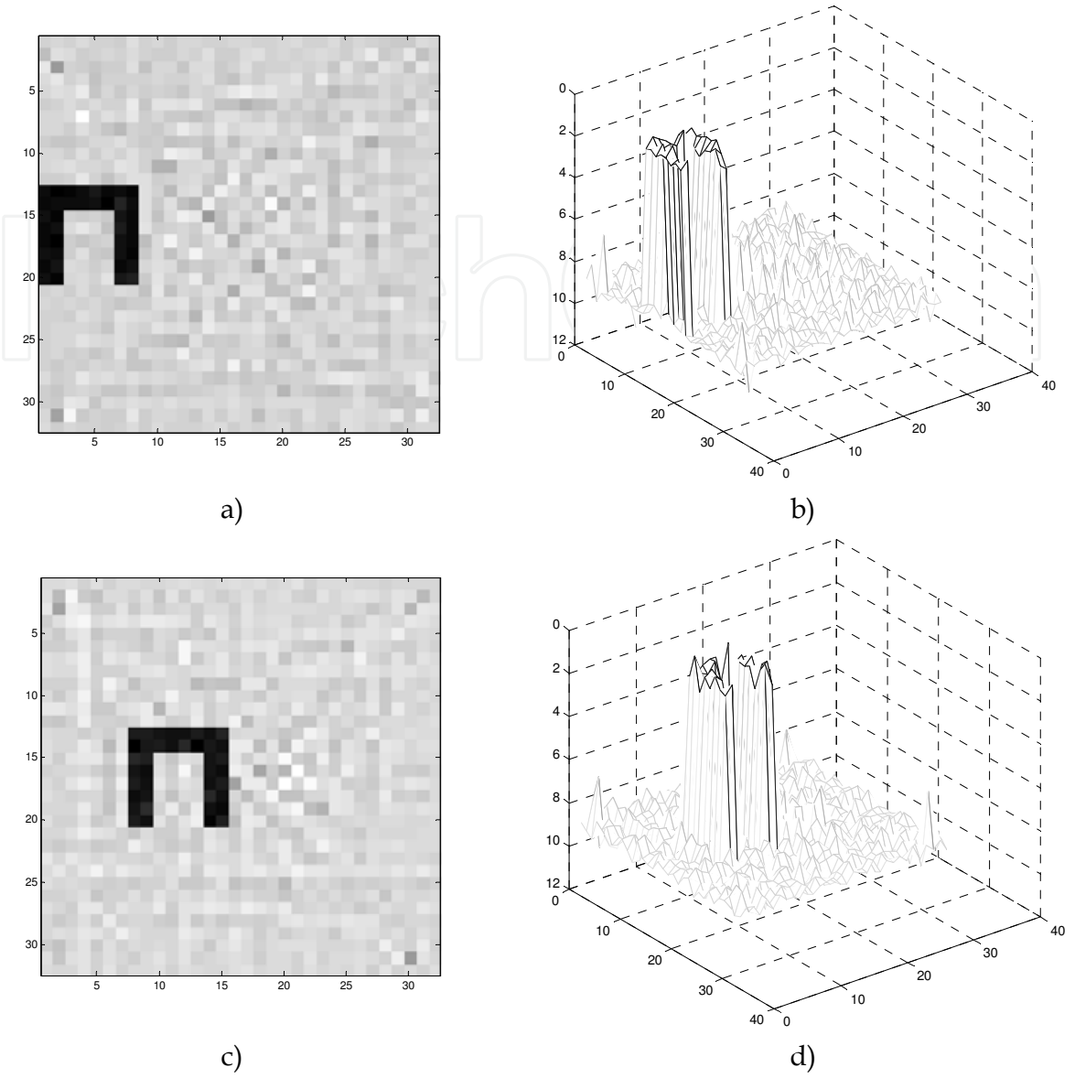

Fig. 11. Two examples of obtained tomography images with their relief plots in W1 (a, b) and W2 (c, d) surfaces used for reconstruction of the flow in 2,5 D

I also have performed calculations for noise polluted data. The noise was generated according to algorithm where the changes in rays flow were achieved through changing the position of transmitters and receivers according to Eq. (33), where in case of noise a random number l_{los} with weight w was added to n_y coordinate l_{los} was within the <0, 1> scope and was calculated by random numbers generator.

$$n_y = n_y + w(l_{los} - 0,5)n_y \tag{33}$$

After that the value was reduced by 0,5 in order to get positive or negative values.
In this case even data with high noise haven't caused big image deformation. It is an essential fact, because real data consists of noise from measurement errors.
The obtained tomography images (Fig. 11) confirm that chosen method gave us images that accurately map tested shape.

3. Conclusion

The calculations with use of the modelling in 2,5D space, give a chance to get results which reflect the phenomenon in the analyzed 3D area, quite accurately (Fig. 9). The obtained results are satisfying and further work should be given the answer for the question, if the proposed method will finding practical application in automotive applications. The simplification of calculations with assuring the sufficient accuracy in making tomography images of analyzed physical phenomenon should succeed in faster obtaining of results. This issue is important because the contemporary tomography is expected to bring real time tomography images of dynamically changing environment.

4. References

Gorodinitsky I.F., George J.S and Rao B.D., (1995), *Neuromagnetic source imaging with FOCUSS: a recursive weighted minimum norm algorithm*, Clinical Neurophysiology, vol. 95, pp. 231-251

Kak A., C., Slaney M. (1999) *Principles of Computerized Tomographic Imaging*, IEEE Press, ISBN: 0-87942-198-3

Kupnik M. (2008) *Ultrasonic Transit-time Gas Flowmeter for Automotive Applications*, VDM Verlag Dr Műller, ISBN: 978-3-639-00789-3

Lawson C. L., Hanson R. J. (1995) Solving Least Squares Problems", *Classics in Applied Mathematics 15*, SIAM

Opieliński K., Gudra T. (2006) *Recognition of external object features in gas media using ultrasound transmission tomography*, Ultrasonics, 44, pp.1069-1076.

Mandard E., Kouame' D., Battault R., Remenieras J. P., Patat F. (2008) *Methodology for Developing a High-Precision Ultrasound Flow Meter and Fluid Velocity Profile Reconstruction*, IEEE Transactions on Ultrasonic, Ferroelectrics and Frequency Control, vol. 55, no.1, pp. 161-171

Polakowski K., Sikora J., Filipowicz F.S. (2007) *SVD for image construction in ultrasound tomography*, The International Conference on "Computer as a Tool" EUROCON, Warsaw, pp. 276-281, a

Polakowski K., Sikora J. (2007) *Visualization and image analysis problems in multipath ultrasonic tomography*, 5th World Congress on Industrial Process Tomography WCIPT5, Bergen, pp. 941-948, b

Polakowski K., Sikora J., Filipowicz F.S. (2007) *Idea of 3D Imaging Based on 2,5D Tomography Reconstruction Approach*; 16th International Conference on Systems Science ICSS'07, Wrocław, vol. 3, pp. 206-211, c

Polakowski K., Sikora J., Filipowicz S.F. (2008) *Computer Methods in Monitoring of Flow Processes in Car Systems*, ZKwE, Poznań, April 14-16, pp. 185-186, a

Polakowski K., Sikora J., Filipowicz S.F., Rymarczyk T. (2008) *Tomography Technology Application for Workflows of Gases Monitoring in The Automotive Systems*, Przegląd Elektrotechniczny, R. LXXXIV, 12/2008, pp. 227-229, b

Roger C. Baker (2005) *Flow Measurement Handbook*, Cambridge University Press, pp. 312-351

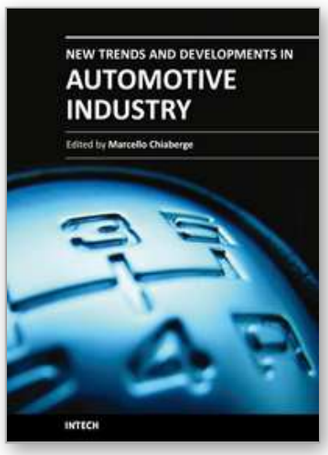

New Trends and Developments in Automotive Industry
Edited by Prof. Marcello Chiaberge

ISBN 978-953-307-999-8
Hard cover, 394 pages
Publisher InTech
Published online 08, January, 2011
Published in print edition January, 2011

This book is divided in five main parts (production technology, system production, machinery, design and materials) and tries to show emerging solutions in automotive industry fields related to OEMs and no-OEMs sectors in order to show the vitality of this leading industry for worldwide economies and related important impacts on other industrial sectors and their environmental sub-products.

How to reference
In order to correctly reference this scholarly work, feel free to copy and paste the following:

Krzysztof Polakowski (2011). Tomography Visualization Methods for Monitoring Gases in the Automotive Systems, New Trends and Developments in Automotive Industry, Prof. Marcello Chiaberge (Ed.), ISBN: 978-953-307-999-8, InTech, Available from: http://www.intechopen.com/books/new-trends-and-developments-in-automotive-industry/tomography-visualization-methods-for-monitoring-gases-in-the-automotive-systems

INTECH
open science | open minds

InTech Europe
University Campus STeP Ri
Slavka Krautzeka 83/A
51000 Rijeka, Croatia
Phone: +385 (51) 770 447
Fax: +385 (51) 686 166
www.intechopen.com

InTech China
Unit 405, Office Block, Hotel Equatorial Shanghai
No.65, Yan An Road (West), Shanghai, 200040, China
中国上海市延安西路65号上海国际贵都大饭店办公楼405单元
Phone: +86-21-62489820
Fax: +86-21-62489821

IntechOpen